Meteorological -High Altitude Laser Optical Spectrometer (HALOS) for atmospheric water and temperature measurements

Anthony Carmine Terracciano[1,2]‡, Chris Fredricksen[3], Francisco Javier Gonzalez[3], Robert E. Peale[3], Subith S. Vasu[1,2,4,5,6], Chelsea Kincaid[1,2], Garrett Mastantuono[1,2], Zachary Rogers[1,2], Abbey Havel[1,2], Andrew DeRusha[1,2], Hamil Patel[1,2], Justin Urso[1,2]

[1] Mechanical and Aerospace Engineering, University of Central Florida, Orlando, Florida; [2] Center for Advanced Turbomachinery and Energy Research, University of Central Florida, Orlando, Florida; [3] Truventic LLC., Orlando, Florida; [4]Physics, University of Central Florida, Orlando, Florida; [5] CREOL, The College of Optics and Photonics, University of Central Florida, Orlando, Florida[6] Florida Space Institute, Orlando, Florida

Keywords: Quantum Cascade Laser, MHz, Flight Instrument, Mid-Infrared, Meteorology, Climate Science, Humidity, CBRN

ABSTRACT

Airborne meteorological instruments are key to climate science, of which understanding cloud formation is an important component. Cloud formation involves the entrainment of air with dissimilar convective, thermal, and humidity properties. Improved understanding of these meteorological parameters can improve forecasting. The National Oceanic and Atmospheric Administration (NOAA) currently relies on outboard sensors with 25 Hz sampling, giving 10 m spatial resolution during nominal fixed wing aircraft flights. Higher-resolution humidity and temperature data are needed. We describe a novel laser absorption-based instrument that can make high sensitivity airborne measurements with 25 cm spatial resolution. The use of mid-infrared (MIR) quantum cascade lasers (QCLs) enables high sensitivity humidity measurements based on strong fundamental vibrations of water vapor. Sampling at 1 MHz (averaged data output exceeding 1 kHz) enables the high spatial resolution from a jet platform that accesses near the ground to 45,000 ft. This technology could be extended using complementary lasers to identify any Chemical, Biological, Radiological, and Nuclear (CBRN) threats, or hazardous material incidents, based on their MIR absorption features. Additional applications could also include highly accurate information for combating wildfires and high-speed identification of anomalous gas-phase species in semiconductor processing.

1. INTRODUCTION & MOTIVATION

Airborne meteorological instruments are key to climate science, of which understanding cloud formation is an important component. Cloud formation involves the entrainment of dissimilar air with unique convective, thermal, and humidity properties [1]. Improved understanding of these parameters will enable the creation of enhanced meteorological models to better inform trans-oceanic transport and severe weather preparedness. Current monitoring platforms and methodologies for atmospheric properties include ground, air, and aerospace instruments [2-4]. Combining these observation techniques with machine learning (ML) provides a superior understanding than the sum of the individual parts [5]. A metrology instrument mounted to an airborne platform would provide higher resolution water vapor concentrations and temperature data. To meet the program needs of the Department of Energy (DOE) or National Oceanic and Atmospheric Administration (NOAA) the University of Central Florida and Truventic LLC have sought to develop a prototype instrument called *High Altitude Laser Optical Spectrometer* (HALOS). Readings from HALOS will include temperature sensitivity on the order of 0.2°C and absolute humidity sensitivity (AH) on the order of 0.010 µmol/m^3 (0.18 mg/m^3) at a data output rate exceeding 1 kHz. HALOS will be a compact platform that is easily integrable in existing DOE or NOAA conventional or remote operated aircraft with either a fixed or rotary-wing. Additional considerations are applied to rapidly integrate the proposed instrument with the existing Gulfstream V aircraft's aperture pads [6].

HALOS will examine conditions across the expected range of temperature, pressure, and supersaturation pertaining to weather conditions through the entire range of the troposphere. Relevant temperature (T), temperature ranges at given altitudes, absolute humidity (ρ_v), relative humidity saturation values (φ), and ambient pressure (P_{amb}) [7-9], Figure 1**.** The

‡ anthony.terracciano@ucf.edu; phone 1 954 793-7563

range of water vapor presented within this figure requires a sensitive detector across nearly 6 orders of magnitude from the 100% relative humidity concentrations at ground level on a warm summer day to the lower limit concentration of 0.6 μmol/m^3 H_2O [11]. The inset within Figure 1 presents a rendering of the portion of the HALOS instrument that will be external to the aircraft. This design incorporates simultaneous (1) short path and (2) multi-pass long path poly spectral sampling of the air, which the aircraft traverses through to reliably quantify any level of water vapor concentration and temperature. Optics and electronics are sealed internally to the aircraft. To minimize obfuscation by water vapor present within the aircraft cabin, free space coupled elements of the emitters and reference laser are to be contained in dry nitrogen (N_2) to eliminate background absorption and ensure negligible *zero*-drift.

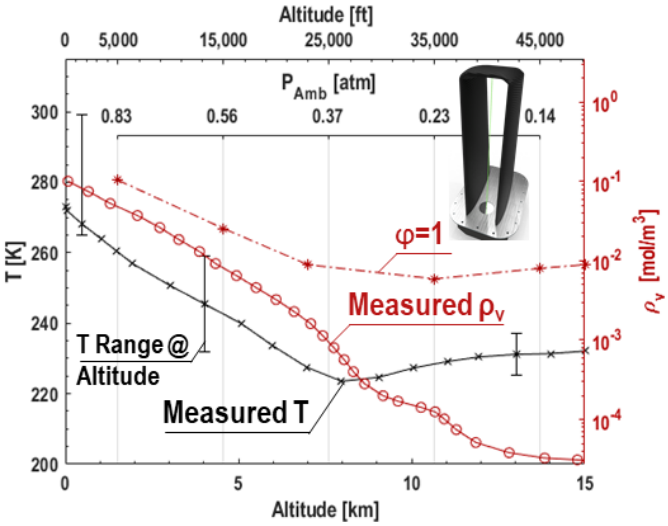

Figure 1. Air-sampling component of HALOS. (right) Temperature and water concentration vs altitude [7-9]. Inset HALOS Rendered model

Innovations within HALOS include a pair of quantum cascade lasers (QCLs) tuned to different fundamental vibrational absorption lines of water vapor in the Mid-IR (MIR) to exploit water's 6.1 μm absorption feature. The lines chosen have an order of magnitude stronger absorption cross section than the overtones traditionally probed by Near-IR (NIR) VECSEL-instruments. As these lines have significantly stronger absorption features, HALOS can provide improved sensitivity and signal-to-noise ratios (SNRs) over the current art. The ratio of the absorption strength for the selected lines probed by HALOS is temperature-dependent, allowing synchronized high-speed measurement of both concentration and temperature. The QCLs are modulated at rates of at least 950 KHz, which exceeds theoretical maximum modulation rates of VECSEL-based hygrometers by ~5x [10]. An innovative analysis method enables the high-speed data rate. A high-speed pressure transducer that measures the free stream static pressure outside of the aircraft will provide synchronous complementary pressure measurements to complete the equation of state. Additionally, other MIR emitters added to this system would enable simultaneous detection of other substances, including chemical weapons [11].

HALOS will enable quantification of the presence of water vapor by exploiting spectral absorption features which dictate how photons at a given wavelength traversing through the gas are attenuated. Using this technique, we have probed for water at high speed in numerous previous efforts [12-14]. In the case of either low species concentration χ_i, or short path length L [cm] [8], absorption of monochromatic light at a particular wavenumber ν [cm^{-1}] is quantified by the Beer-lambert law (1); where α_ν is the absorbance, I and I_0 [W] are the transmitted and incident photon intensities. Absorption is quantified through an exponential relation in which the sample gas is probed and the species absorption cross-section σ_ν [cm^{-1}]. For many gases of interest, σ_ν has been measured and cataloged in various spectral databases such as HITRAN [15]. Conversely, at combinations of high L and/or χ_i, a direct calibration is needed as nonlinear processes dominate [16].

$$\alpha_\nu = -\ln\left(\frac{I}{I_0}\right) = e^{-\sigma_\nu \chi_i L} \qquad (1)$$

2. DESIGN AND PRELIMINARY CALIBRATION

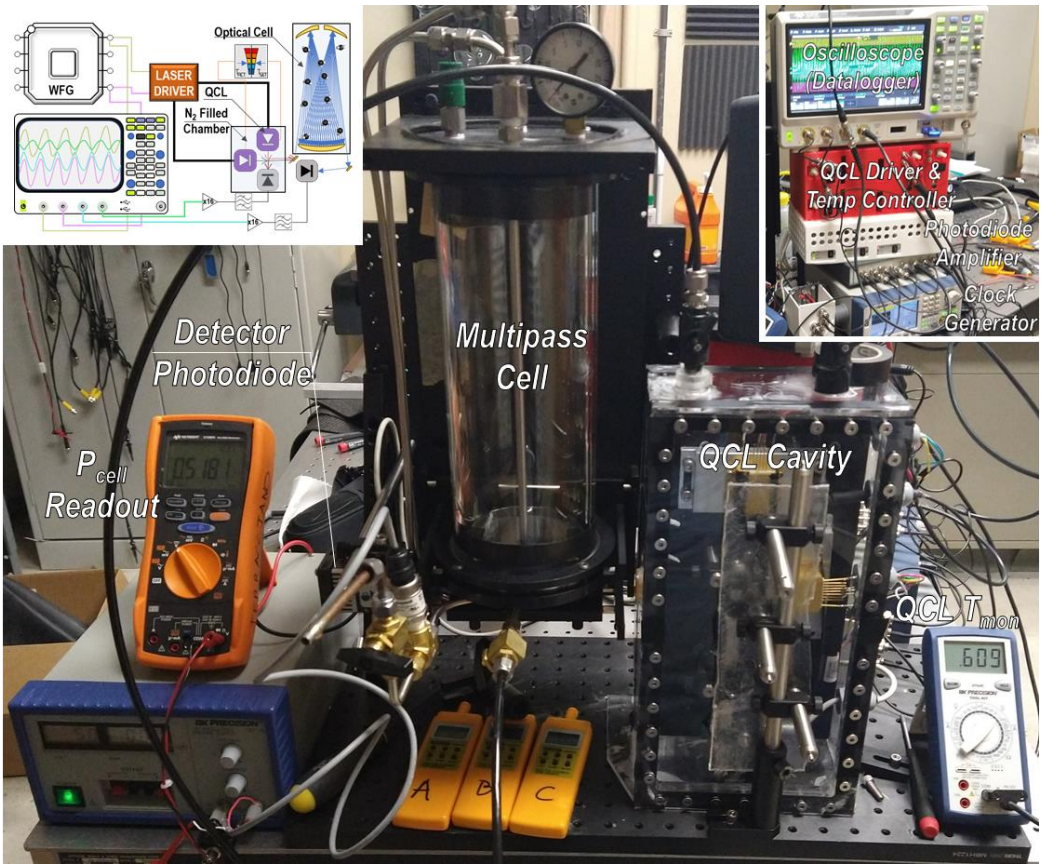

Figure 2: Benchtop prototype of HALOS with inset schematic and electronics control stack.

Figure 2 shows the benchtop version of HALOS. Insets on the left showcase a schematic of the system, while the inset on the right showcases supporting electronics. Within the center of Figure 2 is an enclosed 10 m multipass cell used as the test volume. This chamber has supporting pneumatic hookups to interface with a gas cylinder and high fidelity pressure transducer. Readings from the pressure transducer were calibrated against high accuracy Baratrons to ensure accurate voltage conversion, obtained from a Keysight multimeter as a digital display to pressure within the multipass cell. We have calibrated the transducer used within this work to be accurate to ± 0.13 kPa. The cell may be evacuated, purged, or filled with N_2 and a known water vapor concentration in ppmv. The QCL Cavity (Figure 2) is constructed from plexiglass using acrylic cement, butyl rubber gaskets, and a ZnSe window for the output beam. Both QCLs, a beam splitter, and a reference detector housed this anhydrous cavity. This volume is filled with continuously flowing dry N_2, ensuring "zero" water vapor within the cavity. Thus affording low jitter and drift in the reference detector output, which provides a value computationally analogous to $\boldsymbol{I_0}$ [17].

The electronics stack (Figure 2 inset) contains several elements for data logging and regulating photodiodes/lasers. Data is logged using a four-channel oscilloscope (Teledyne T3DSO2104A) and saved to a USB drive via a .csv file. A two-channel waveform generator (BK Precision 4055B) (WFG) generates sine waves at 950 kHz and 1 MHz. Each of the signals from the WFG is split; one of the split signals are fed to the oscilloscope for clock reference while the other goes to the QCL driver to enable modulation. The custom QCL driver system shown in Figure 2 enables the regulation of temperature and controlling current and voltage to the laser diodes. Temperature stabilization is achieved to within ±0.01°C of a steady-state using a closed-loop PID controller. Signals from the reference and measurement photodiodes are sent through a band pass filter to attenuate the DC and high frequency noise components before amplification (Stanford Research Systems SR 440), with a programmed gain value of 12 dB and logging on the oscilloscope which has 10-bit voltage resolution across the selectable full scale range. Subsequent waveform analysis was then conducted in Matlab.

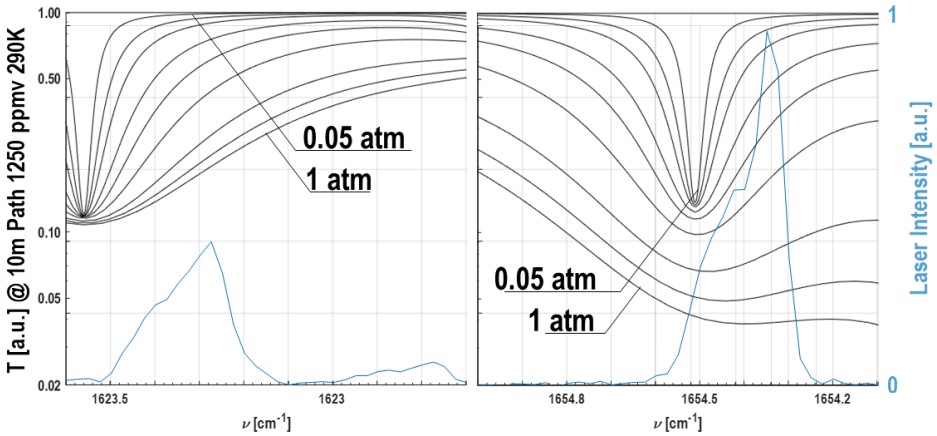

Figure 3: QCL output (blue) and Transmittance through a 10m water vapor at 296 K and 1250 ppm concentration across a range of pressures.

Lasing spectral output calibration was conducted to ensure sufficient ability to probe water vapor at two wavelengths 1623 cm^{-1} and 1654 cm^{-1}. This was achieved via measuring laser output using a Fourier Transform Interferometer (FTIR) (Bomem DA8) with a L-N_2 cooled detector at a 0.25 cm^{-1} resolution. During the tuning process, output of the laser was controlled via the parametric adjustment of a DC threshold voltage on the controller; this was set to just below the "on" threshold for each of the two QCLs. An additional voltage to control wavelength was then imposed from the upper and lower bounds of the sine wave excitation sources; this value was strategically chosen to provide the largest dynamic range for each QCL between the current limit of approximately 300 mA and the threshold voltage. Additional wavelength control was achieved via PID regulation of the QCL emitter temperature. Laser line selection was identified via the transmittance line shapes (black curves), and was calculated from HITRAN [16], shown in Figure 3. These transmittance data correspond to 10 m pathlengths 1250 ppmv H_2O at 296K and variable pressure from 1 atm to 0.05 atm, which exceeds the range expected by the Gulfstream V flight ceiling. From the transmittance plots, line narrowing occurs, and thus the absorbance at a single wavelength decreases faster than linearly with decreasing concentration. Conversely, due to the concentration decrease, the transmittance at the line center remains nearly constant. Suggesting that the optimum wavelength for measuring water concentration from the absorption coefficient and line shape function is slightly biased off-peak but not too far out into the wings. These findings will be further implemented in subsequent HALOS development efforts, thus affording us the maximum dynamic range.

Figure 4 presents an overlay of the time-averaged spectra, black, recorded on an FTIR, with the time-dependent detector output during a modulation cycle blue following bandpass filtering and amplification. The 1623 cm^{-1} QCL is modulated at 950 kHz and the 1654 cm^{-1} QCL is modulated at 1 MHz. Channel spacing was selected based on parametric analysis of signal overlap *sans*-filtering. The figure shows a near congruent intensity profile as both a function of time and wavelengths.

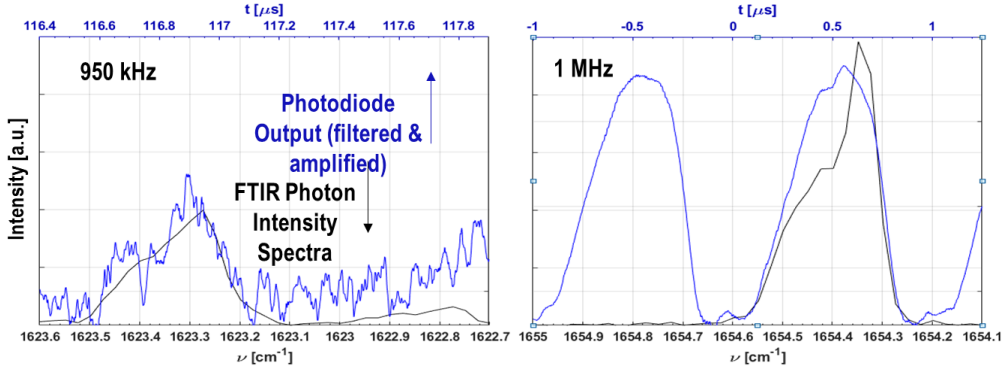

Figure 4: Detected laser intensity vs time (blue) and laser spectrum (black). Intensity for both plots is consistent on a geometric amplitude.

From the sinusoidal modulation of intensity about some bias current concurrently with a wavelength modulation, it is possible to mathematically represent the intensity and time expressions through a Fourier series (2) and concurrently a wavelength and time expression through a Fourier series (3). Thus, it is possible to relate wavelength and intensity of the zero absorbance function by relating equations (2) and (3) [10]. Where wavelength λ is a function of some centerline wavelength λ_0 and each term in the Fourier series has a specific amplitude λ_n and phase φ_n. at the modulation frequency f_0. Similarly for the intensity function, there is some I_0 centerline value with additional harmonic amplitudes and phases I_n and ϕ_n, respectively. As there is cyclic nature of these laser intensity and wavelength, noise can be reduced through considering a sample of fixed number of cycles via a time-dependent measure at such high repetition rates. Then transform the signals into the frequency domain for subsequent processing.

$$\lambda(t) = \lambda_0 + \sum_n \lambda_n \cdot \sin\left(n \cdot 2 \cdot \pi \cdot t \cdot f_0 + \varphi_n\right) \quad (2)$$

$$I(t) = I_0 + \sum_n I_n \cdot \sin\left(n \cdot 2 \cdot \pi \cdot t \cdot f_0 + \phi_n\right) \quad (3)$$

3. BENCHTOP VALIDATION

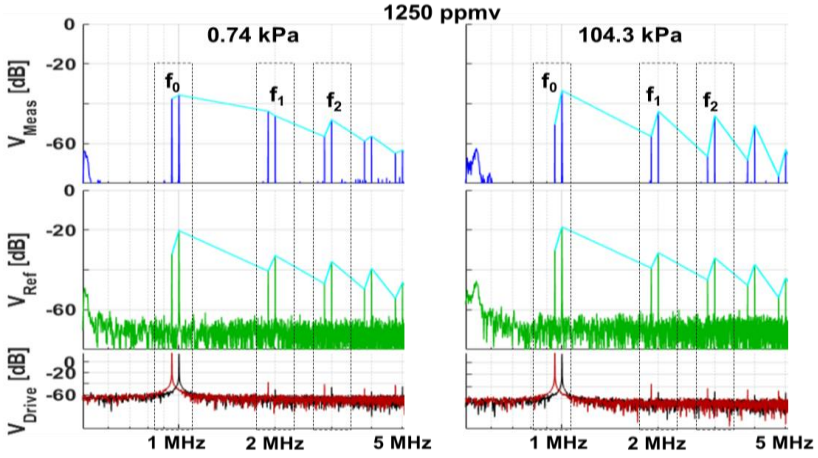

Figure 5. FFT of drive voltage and measured sample and reference signals.

Figure 5, from bottom to top presents the FFT of the QCL modulation voltage (red and black), the reference signal (green), and the sample signal (dark blue) across two pressures 0.74 kPa and 104.3 kPa at an absolute H_2O concentration of 1250 ppmv and 20±3°C was maintained constant during tests. The left plots correspond to a pressure reached above 50,000' while the right plots correspond to sea level measurements. The FFT demodulation provides distinct peaks at the 1f fundamentals 0.95 and 1.00 MHz. The drive voltage spectrum shows mainly these 1f fundamentals. Both sample and reference signals show strong harmonics 2f and beyond. As these harmonics appear in both reference and measurement channels, we can ascertain that these are dependent upon the emitted wavelengths of the QCL and intensity variations are the result of absorption from water. The relative strength of the harmonics is nearly the same in both channels, means that they are due primarily to the large intensity modulation and the non-linear dependence of laser intensity on drive current.

On both the V_{Ref} and V_{Meas} plots within Figure 8, light blue lines are drawn between each of the peaks due to the intensity finding algorithm we have developed to simplify the practical use of the FFT and highlight the successive highest intensity values. The relative magnitude between each modulation frequency can be computed as a vector to identify characteristics within the flow. Comparing the sample signals at the two pressures shows that at ~1 atm pressure the 0.95 MHz sample signal is reduced more strongly than the 1.00 MHz signal; this is by design as a result of water absorption and enables ***HALOS*** to scan an extensive dynamic range with ease. The successive harmonics in the sample signal behave similarly, as expected for an intensity-independent absorption process. The sample signals go down with increasing water

concentration is another indication that wavelength modulation is unimportant. If there only wavelength modulation and there was no water, there would be no harmonics in transmittance. Then if water concentration increased, so would the non-linearities in the wavelength dependence of transmittance, and harmonics would *increase*.

Within Figure 6, an expanded data set containing information within Figure 8 is presented in which pressure of the gases is changed within the sample cell while maintaining temperature 20±3°C and water vapor concentration 1250 ppmv. This is by design of the instrument to expand the sensor's dynamic range of sensing concentration on the 1623 cm^{-1} under high water vapor conditions. As can be seen in the f_0 trace, there is a near linear increase in the ratio of the V_{Meas}/V_{ref} as pressure within the cell increases. The higher linearity observed in the 1654 cm^{-1} line is attributable to the relative strength of the absorption feature at that wavelength. However, when examining the f_1 harmonic, it can be seen that the relative slope is more pronounced and thus, the higher harmonic signal analysis increases the instrument's dynamic range.

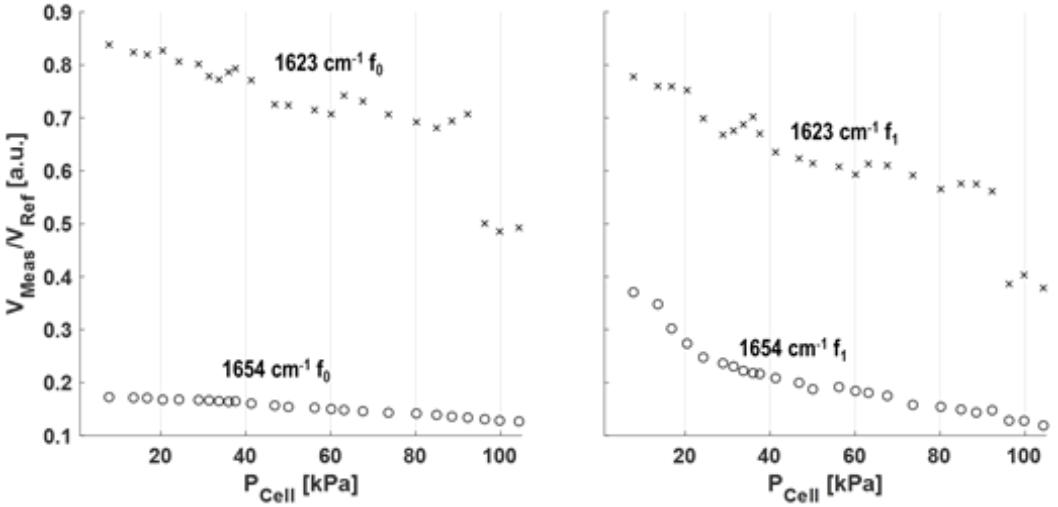

Figure 6. Pressure dependence of f_0 and f_1 signal ratios with water fixed at 1250 ppmv.

4. CONCLUSION AND FUTURE WORKS

A novel laser absorption-based instrument that can make high sensitivity airborne measurements with 25 cm spatial resolution was presented. The use of mid-infrared (MIR) quantum cascade lasers (QCLs) enabled high sensitivity humidity measurements based on strong fundamental vibrations of water vapor. Sampling at 1 MHz (averaged data output exceeding 1 kHz) enabled high spatial resolution from a jet platform that accesses near sea level to 45,000 ft. Future works for this effort include repacking of the optical system and hardening the components for airborne proving demonstrations. Additionally integration with other data manipulation methodologies such as a real-time interface will be necessary to enhance the user experience of the instruments.

ACKNOWLEDGMENTS AND DISCLOSURE

The authors would like to thank Max Tafoya for his contributions of laboratory preparation. Chris Fredricksen and Robert Peale have an interest in Truventic LLC and may benefit financially from the results of the research presented here. This material is mainly based upon work supported by the U.S. Department of Energy, Office of Science, Office of Basic Energy Sciences under Award Number DE-SC0021488. This work also benefited from the matching support provided by the Florida High Tech Corridor Council (FHTCC).

REFERENCES

[1] T. Raatikainen *et al.*, "Worldwide data sets constrain the water vapor uptake coefficient in cloud formation," *Proceedings of the National Academy of Sciences*, vol. 110, no. 10, pp. 3760-3764, 2013.

[2] S. Kotthaus, C. H. Halios, J. F. Barlow, and C. Grimmond, "Volume for pollution dispersion: London's atmospheric boundary layer during ClearfLo observed with two ground-based lidar types," *Atmospheric Environment*, vol. 190, pp. 401-414, 2018.

[3] N. Ferlay, T. J. Garrett, and F. Minvielle, "Satellite observations of an unusual cloud formation near the tropopause," *Journal of the Atmospheric Sciences*, vol. 71, no. 10, pp. 3801-3815, 2014.

[4] D. Vignelles *et al.*, "Balloon-borne measurement of the aerosol size distribution from an Icelandic flood basalt eruption," *Earth and Planetary Science Letters*, vol. 453, pp. 252-259, 2016.

[5] M. Alshaye, F. Alawwad, and I. Elshafiey, "Hurricane Tracking Using Multi-GNSS-R and Deep Learning," in *2020 3rd International Conference on Computer Applications & Information Security (ICCAIS)*, 2020: IEEE, pp. 1-4.

[6] (2008). *NSF / NCAR Gulfstream V Investigator's Handbook*.

[7] C. Tomasi *et al.*, "Mean vertical profiles of temperature and absolute humidity from a 12-year radiosounding data set at Terra Nova Bay (Antarctica)," *Atmospheric research*, vol. 71, no. 3, pp. 139-169, 2004.

[8] A. C. Terracciano *et al.*, "Hazardous gas detection sensor using broadband light-emitting diode-based absorption spectroscopy for space applications," *New Space*, vol. 6, no. 1, pp. 28-36, 2018.

[9] "Altitude above Sea Level and Air Pressure." The Engineering Toolbox. https://www.engineeringtoolbox.com/air-altitude-pressure-d_462.html (accessed 2020).

[10] J. Chen, "Compact laser-spectroscopic gas sensors using vertical-cavity surface-emitting lasers," Technische Universität München, 2011.

[11] S. Neupane, R. Peale, and S. Vasu, "Infrared absorption cross sections of several organo-phosphorous chemical-weapon simulants," *Journal of Molecular Spectroscopy*, vol. 355, pp. 59-65, 2019.

[12] Z. Loparo, K. Thurmond, A. Lyakh, and S. Vasu, "Novel diagnostic technique for ultra-fast, simultaneous temperature and concentration measurements for harsh hypersonic flows," in *23rd AIAA International Space Planes and Hypersonic Systems and Technologies Conference*, 2020.

[13] K. Thurmond, I. Dunn, K. A. Ahmed, and S. Vasu, "Measurements of H_2O, CO_2, CO, and static temperature inside rotating detonation engines," in *AIAA Scitech 2019 Forum*, 2019, p. 0747.

[14] Z. Loparo *et al.*, "Towards a laser-absorption technique for ultra-fast, simultaneous temperature and concentration measurements inside pressure gain combustion devices," in *AIAA Propulsion and Energy 2019 Forum*, 2019, p. 4040.

[15] C. Hill, I. E. Gordon, R. V. Kochanov, L. Barrett, J. S. Wilzewski, and L. S. Rothman, "HITRANonline: An online interface and the flexible representation of spectroscopic data in the HITRAN database," *Journal of quantitative spectroscopy and radiative transfer*, vol. 177, pp. 4-14, 2016.

[16] K. Thurmond, Z. Loparo, W. Partridge, and S. S. Vasu, "A light-emitting diode-(LED-) based absorption sensor for simultaneous detection of carbon monoxide and carbon dioxide," *Applied spectroscopy*, vol. 70, no. 6, pp. 962-971, 2016.

[17] B. Koroglu, O. M. Pryor, J. Lopez, L. Nash, and S. S. Vasu, "Shock tube ignition delay times and methane time-histories measurements during excess CO_2 diluted oxy-methane combustion," *Combustion and flame*, vol. 164, pp. 152-163, 2016.